IEEE Access
Multidisciplinary | Rapid Review | Open Access Journal

Received September 26, 2016, accepted November 10, 2016, date of publication November 29, 2016,
date of current version January 4, 2017.

Digital Object Identifier 10.1109/ACCESS.2016.2633304

A Wearable Inertial Measurement System With Complementary Filter for Gait Analysis of Patients With Stroke or Parkinson's Disease

HSING-CHENG CHANG[1], YU-LIANG HSU[1], SHIH-CHIN YANG[2], (Member, IEEE), JUNG-CHIH LIN[3] AND ZHI-HAO WU[1]

[1]Department of Automatic Control Engineering, Feng Chia University, Taichung 40724, Taiwan
[2]Department of Mechanical Engineering, National Taiwan University, Taipei 10617, Taiwan
[3]Department of Integrated Chinese and Western Medicine, Chung Shan Medical University Hospital, Taichung 402, Taiwan

Corresponding author: H. C. Chang (hcchang@fcu.edu.tw)

ABSTRACT This paper presents a wearable inertial measurement system and its associated spatiotemporal gait analysis algorithm to obtain quantitative measurements and explore clinical indicators from the spatiotemporal gait patterns for patients with stroke or Parkinson's disease. The wearable system is composed of a microcontroller, a triaxial accelerometer, a triaxial gyroscope, and an RF wireless transmission module. The spatiotemporal gait analysis algorithm, consisting of procedures of inertial signal acquisition, signal preprocessing, gait phase detection, and ankle range of motion estimation, has been developed for extracting gait features from accelerations and angular velocities. In order to estimate accurate ankle range of motion, we have integrated accelerations and angular velocities into a complementary filter for reducing the accumulation of integration error of inertial signals. All 24 participants mounted the system on their foot to walk along a straight line of 10 m at normal speed and their walking recordings were collected to validate the effectiveness of the proposed system and algorithm. Experimental results show that the proposed inertial measurement system with the designed spatiotemporal gait analysis algorithm is a promising tool for automatically analyzing spatiotemporal gait information, serving as clinical indicators for monitoring therapeutic efficacy for diagnosis of stroke or Parkinson's disease.

INDEX TERMS Inertial sensing, gait analysis, complementary filter, sensor fusion, stroke, Parkinson's disease.

I. INTRODUCTION

According to the World Health Organization (WHO) reports, neurological disorders have been one of the substantial public health threats, such as dementia, epilepsy, stroke and Parkinson's disease (PD) [32]. Among these neurological disorders, stroke is the main noncommunicable disease, which has been reported worldwide as the second leading cause of death [34], while Parkinson's disease is recognized as a chronic neurodegenerative disorder, with a crude incidence varied from 4.5 to 19 per 100,000 population per year [32]. As reported in [19], around 17 million people suffered strokes in 2010 where three-fourths of the survivors became disable. Additionally, around 52∼85 % hemiplegic patients were able to recover their walking capacity via rehabilitation participation. However, their gait was characterized by alterations in spatiotemporal parameters, such as reduced walking speed and gait symmetry [2], [19], [36]. Therefore, the recovery of walking capacity in stroke rehabilitation focuses on the assessment and treatment of gait disorders. In addition to stroke, the expected number of patients with PD will rise more than 9 million in year of 2030, as reported in [6] and [9]. It results in alterations in kinematic and kinetic walking patterns, such as increased stride-to-stride variability, reduced stride velocity, and reduced step length [1], [17], [25]. Furthermore, some clinical reports indicated that gait disorders decrease the mobility and increase the risk of falling for patients with stroke or PD [4], [26], [29].

Gait analysis is widely utilized in monitoring human gait movement affected by stroke rehabilitation [24], [36] and PD [7], [9]. To analyze gait information of patients with stroke or PD, many instrumented walkway systems, such as GaitRite system and CIR system, are widely used to recognize gait patterns for clinical experiments. In addition, some optical capture systems, such as Codamotion optical

tracking system and VICON MX motion capture system, are also frequently utilized to capture walking motion and calculate gait parameters. To name a few, Boudarham *et al*. [2] analyzed stroke patients' spatiotemporal and sagittal kinematic parameters, such as gait velocity, stride time, stride length, cadence, step width, step length, stance phase time, swing phase time, double support time, and sagittal hip, knee, and ankle kinematic waveforms, by using the OrthoTrack 6.5 software-based motion analysis system. Sofuwa *et al*. [27] utilized the Vicon three dimensional motion capture system composed of 8 infrared sensitive cameras and 3 AMTI forceplates mounted on an 8m walkway to analyze walking velocity, stride length, cadence, double support, single support, and range of motions (ROMs) of ankle, knee, hip, and pelvis joints between healthy control (HC) and PD subjects. However, the drawbacks of the walkway instruments and optical capture systems are expensive, constrained to a laboratory environment, and require more spaces, which causes these methods are not used in clinical applications or home set-up widely.

Over the past decades, many inertial-sensor-based gait analysis systems have been developed to analyze spatiotemporal gait patterns for normal human [16], [31], stroke subjects [4], [10], [22], [24], [29], [30], [36], and PD patients [1], [3], [7], [8], [21], [26], [29], [30]. For example, Mizuike *et al*. [22] analyzed the correlation between the gait parameters and functional recovery using the acceleration signals. These findings indicated that the raw RMS and autocorrelation (AC) in stroke were significantly lower than those in matched healthy elderly. In addition, for stroke patients, their normalized RMS values were significantly higher than the HCs. Guo *et al*. [10] attached the inertial sensors to the thigh, shank, and dorsum of foot of the participants for accurately measuring the angle amplitudes of initial contact, toe off, and knee flexion/extension in the sagittal plane, which were much higher in the HCs than in the hemiplegia group. Demonceau *et al*. [7] mounted a trunk accelerometer system on the PD subjects' lower back nearby the body center of mass for extracting spatiotemporal gait information, such as walking speed, stride length, cadence, regularity, symmetry, and mechanical powers. The results showed that stride length normalized to height in PD patients is significantly lower than HCs. Rezvanian and Lockhart [26] employed the continuous wavelet transform (CWT) of the accelerometer data to define an index for correctly detecting freezing of gait (FOG) of the PD patients. Din *et al*. [8] utilized an accelerometer mounted on the lower back to obtain the step time, stance time, swing time, step length, and step velocity in patients with PD. Bamberg *et al*. [1] and Morris [21] developed the GaitShoe to measure the gait patterns of PD and HC groups, which integrated two dual-axis accelerometers for determining the velocity and displacement, two types of gyroscopes for calculating the pitch angle of the foot, force sensitive resistors (FSRs) for detecting the stride timing and weight distribution, two polyvinylidene fluoride (PVDF) strips for finding heel strike time and toe off time, a bidirectional bend sensor for evaluating plantarflexion and dorsiflexion angles, a multielectrode electric-field imaging device for detecting distances above ground, and an ultrasound sensor for obtaining board to board distances and angles between feet. PD patients showed differences in smaller pitch angles, shorter stride length, longer stride time, and larger percent stance time than HCs.

Based on the abovementioned literature review, gait analysis and spatiotemporal gait parameters can be used to provide an effective assessment method for healthcare and medical treatment for patients with stroke or PD. Hence, a self-developed and low-cost wearable inertial measurement system (IMS) and its associated spatiotemporal gait analysis algorithm is developed in this paper for the purpose to provide accurate gait information detection without any space limitation. The wearable IMS consists of a microcontroller, a triaxial accelerometer, a triaxial gyroscope, and an RF wireless transmission module. The advantages of the proposed IMS include low cost, small size, low power consumption, and without any space limitation and supplementary instrument. Participants can mount the IMS on their foot while walking along a straight line of 10 m at normal speed without any external motion capture techniques. Accelerations and angular velocities generated from walking motions and measured by the accelerometer and gyroscope are transmitted to a computer via the wireless module. When participants mount the wearable IMS on their foot during walking, spatiotemporal gait information can be extracted by a spatiotemporal gait analysis algorithm which is comprised of the procedures of inertial signal acquisition, signal preprocessing, gait phase detection, and ankle ROM estimation. In order to minimize the cumulative error of the inertial signals, a sensor fusion technique based on a complementary filter is utilized to fuse acceleration and angular velocity signals for subsequent correction of the ankle ROM estimation. The objective of this study is to find out the characteristic gait parameters to be served as assistive indicators for discriminating between the healthy elderly and stroke or PD groups effectively by using the inertial signals with the complementary filter during walking.

The remainder of this paper is organized as follows. In Section II, the demographics and participant characteristics, apparatus, and procedures are described in detail. Subsequently, the spatiotemporal gait analysis algorithm, composed of inertial signal acquisition, signal preprocessing, gait phase detection, and complementary filter based ankle ROM estimation, is presented in Section III. Section IV validates the effectiveness of the proposed wearable IMS and its associated spatiotemporal gait analysis algorithm, and provides the results and discussions. Finally, conclusions are summarized in Section V.

II. EXPERIMENTAL SETUP

A. PARTICIPANTS

In this study, for gait analysis tests, all 24 participants were referred to the Department of Integrated Chinese and Western

Medicine at Chung Shan Medical University Hospital, with 4 stroke patients (three hemiplegia and one diplegia, the age ranges between 38-57, mean ± S.D.: 51.50±7.89 years), 5 PD patients (the age ranges between 66-87, mean ± S.D.: 76.20±8.64 years), and 15 HCs (the age ranges between 51-80, mean ± S.D.: 68.47±8.03 years) according to the professional diagnosis. In addition, the mean onset ages of total stroke was 1.40±0.42 years, and the time from onset of PD patient is 9.85±0.56 years. In this paper, all the statistical tests were performed with SPSS 16.0 software. The significant differences of all the statistical results between each group were performed by using analysis of variance (ANOVA) test. A significant difference between HCs and stroke or PD patients is concluded when the p-value < 0.05. Subjects were excluded from participants in this paper if their body mass index (BMI) scores > 35, were unable to walk at least 10 m without assistance, reported pain sufficient to affect their walking, history of falls in the past year, had Alzheimer's disease, or orthopedic surgery in the past year. The demographics of the participants for the gait analysis tests are summarized in Table 1. The study protocol was approved by the University Human Ethics Committee and informed consent has been acquired from all subjects.

TABLE 1. Participant characteristics for gait analysis tests.

Parameters	Stroke N = 4	PD N = 5	HC N = 15
Men/Women (n)	2/2	4/1	8/7
Height (cm)	162.25±6.22	161.70±9.54	161.43±8.47
Weight (kg)	59.34±11.32	68.00±7.58	66.08±8.31
BMI (kg/m^2)	22.39±3.67	23.56±2.32	23.40±2.28
Age (years)	51.50±7.89	76.20±8.64	68.47±8.03
Time from Onset (years)	1.40±0.42	9.85±0.56	-

B. APPARATUS

In this paper, we develop a wearable IMS which includes a foot-mounted IMS module and a human-computer interface (HCI) for online spatiotemporal gait analysis. The foot-mounted IMS module is composed of a six-axis inertial sensor (MPU-6050), a microcontroller (ATmega 328), an RF wireless transmission module (nRF24L01), and a power supply circuit. The six-axis inertial sensors (MPU-6050) consists of a triaxial accelerometer, a triaxial gyroscope, and 16 bit analog to digital converters (ADCs), which are used to simultaneously detect the accelerations and angular velocities generated from walking movements in a 3-dimensional (3D) space and output the digital measurement signals. The triaxial accelerometer can measure the gravitational and motion accelerations of walking motions and possesses a linear acceleration full scale of ±2, ±4, ±8, and ±16 g, with data output rate from 4 to 1000 Hz for all axes. The triaxial gyroscope simultaneously detect the X-, Y-, and Z-axis angular rates of the IMS module mounted on participants' foot during walking and possesses a full scale of ±250, ±500, ±1000, and ±2000 °/s, with data output rate from 4 to 8000 Hz for all axes. In this paper, the sensitivity and measure range of the accelerometer are 4096 LSB/g and ±8 g, while which of the gyroscope are 16.4 LSB/°/s and ±2000 °/s. Table 2 represents characteristics of the sensors embedded in the MPU-6050. The microcontroller (ATmega 328) of the IMS module is responsible to collect the digital signals generated from the accelerometer and gyroscope through an I^{2}C interface and to connect to the RF wireless transceiver through an SPI interface. The RF wireless transceiver (nRF24L01) is used to transmit wirelessly the accelerations and angular velocities to a HCI for further real-time signal processing and analysis. The sampling rate of the measured inertial signals is set at 100 Hz. The power supply circuit is composed of a Li-ion battery, a Li-ion battery charging module, and regulators, which provides the power consumption for the IMS module. The battery of the IMS module is replaceable and rechargeable. The schematic diagram of the wearable IMS module hardware system is shown in Fig. 1. The overall power consumption of the hardware device is 57 mA at 3.7 V. The weight and size of the IMS module are 42.2 g and 60 mm × 50 mm × 20 mm, as shown in Fig. 2. Therefore, the wearable device possesses the fundamental requirements for daily monitoring: low power consumption, lightness, small size, and sensing capability.

TABLE 2. The specification of MPU-6050.

Parameters	Accelerometer	Gyroscope
Sensitivity	4096 LSB/g	16.4 LSB/°/s
Resolution	16 bit	16 bit
Supply voltage	2.375~3.46 V	2.375~3.46 V
Output interface	I²C	I²C
Measuring range	±8 g	±2000 °/s

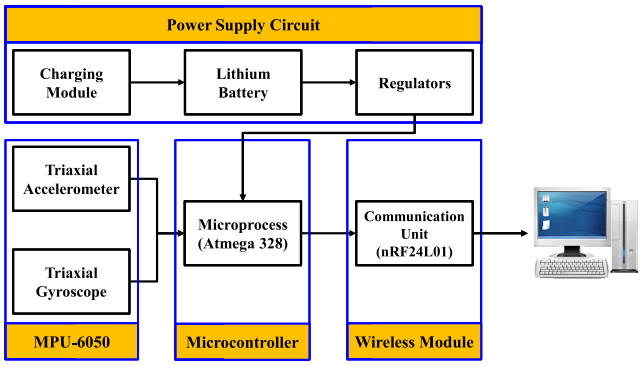

FIGURE 1. Schematic diagram of the wearable multi-axis inertial measurement module.

C. PROCEDURE OF EXPERIMENTS

The wearable IMS module was attached on the foot of the participants in the gait analysis tests. For the hemiplegic stroke patients, the only one sensor module was attached on their abnormal side; for the diplegic patient, HCs, and PD patients, sensor modules were attached on their feet. The wearable IMS modules were mounted on the dorsum of feet as shown in Fig. 3(a). The segment coordinate system of the IMS module is shown as Fig. 3(b). The intersection of the X and Z axes can

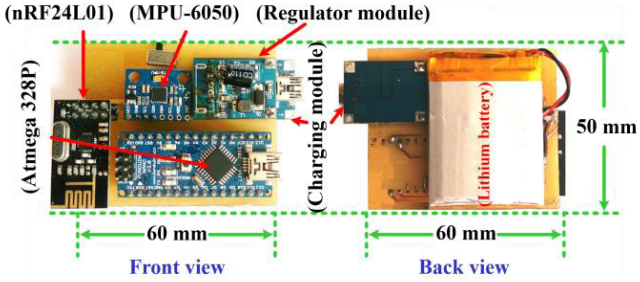

FIGURE 2. The proposed wearable multi-axis inertial measurement module.

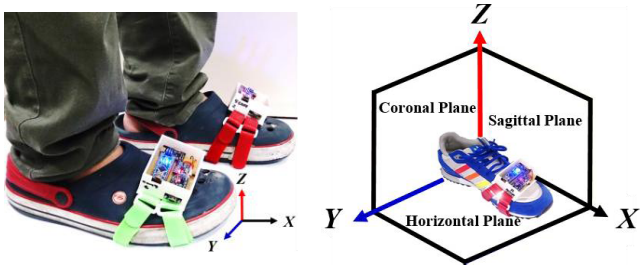

FIGURE 3. Feet attached the wearable multi-axis inertial measurement modules for gait analysis (a) The segment coordinate system. (b) The sagittal, coronal, and horizontal planes.

be defined as the sagittal plane and the Y axis is orthogonal to the sagittal plane. The participants were demanded to walk along a straight line of 10 m on the second floor of the Chung Shing Branch Building at Chung Shan Medical University Hospital (10 m walking test [13], [36]). During the walks, all participants were asked to walk at normal speed and repeated the walking trails one more time after an interval, over a period of 2 min. Each participant were accompanied by an assistant to minimize the risk of falls. The researcher must remain out of the subjects' sight to avoid the interferences resulted from his/her presence to the walking test causing unnecessary cues for the subjects' movement.

III. SPATIOTEMPORAL GAIT ANALYSIS ALGORITHM

A spatiotemporal gait analysis algorithm has been developed in this study to automatically acquire the spatiotemporal gait parameters by using the acceleration and angular velocity signals, and is composed of the following procedures: 1) inertial signal acquisition, 2) signal preprocessing, 3) gait phase detection, and 4) complementary filter based ankle ROM estimation. First, the foot-mounted IMS module transmitted the inertial signals generated from foot movements during walking, which are measured by the triaxial accelerometer and gyroscope, to the proposed HCI via the RF wireless transceiver. Second, the sensitivity and offset errors of the sensors and the influence of users' unconscious trembles and walking friction are calibrated and eliminated through the signal preprocessing procedure. Third, the signal vector magnitude (SVM) and Y-axis (in the sagittal plane direction) of the filtered angular velocity signals are used to detect the toe-off and heel-strike points during walking movements for further calculating gait parameters. Finally, the complementary filter based sensor fusion method is utilized to accurately estimate the ankle angles in the sagittal plane during walking movements. The block diagram of the proposed spatiotemporal gait analysis algorithm is shown in Fig. 4. We now introduce the detailed procedures of the proposed spatiotemporal gait analysis algorithm.

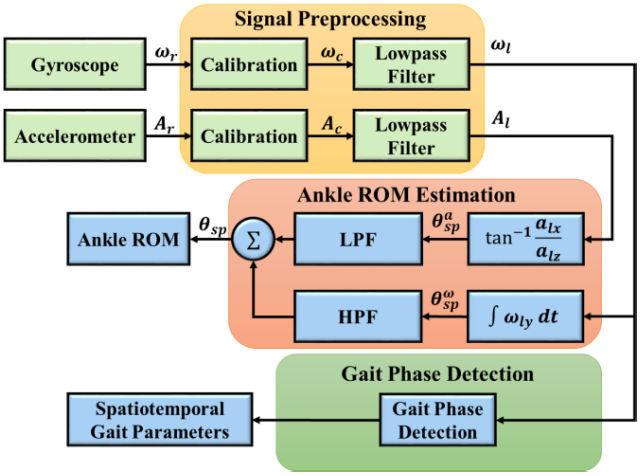

FIGURE 4. The proposed spatiotemporal gait analysis algorithm.

A. SIGNAL PREPROCESSING

This signal preprocessing procedure is a crucial procedure after inertial signal acquisition, which is composed of calibration and lowpass filtering for removing the efforts of the sensors' error sources and user's unconscious trembles and walking friction.

1) CALIBRATION

The goal of the calibration of the accelerations and angular velocities is to reduce errors of sensitivity and offset from the raw measurements. For the accelerometer calibration, we place each axis of the triaxial accelerometer alternately upward and downward to align with the Earth's gravity which can be only measured by the accelerometer when the foot-mounted IMS module is stationary. Then, we can obtain the scale factor ($\mathbf{SF}_{acc}$) and offset ($\mathbf{O}_{acc}$) for each axis of the accelerometer. For the calibration of the triaxial gyroscope, we utilize the sensitivity value represented in the datasheet to be the scale factor ($\mathbf{SF}_{gyro}$) for each axis of the gyroscope. Additionally, the mean values of the angular velocities in each axis at the beginning are used to be the offset ($\mathbf{O}_{gyro}$) for each axis of the triaxial gyroscope, which should be zero when the foot-mounted IMS module is stationary. Subsequently the scale factor ($\mathbf{SF}$) and offset ($\mathbf{O}$) of the sensors are utilized to obtain the calibrated measurements of the sensors as equation (1).

$$\mathbf{S}_c = \mathbf{SF} \times \mathbf{S}_r + \mathbf{O}, \tag{1}$$

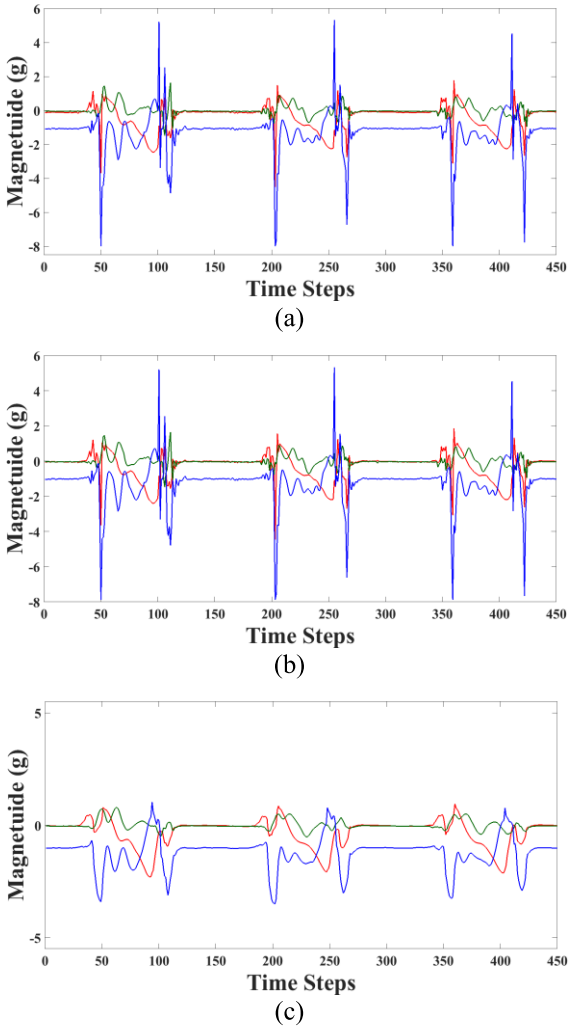

FIGURE 5. Signal preprocessing of accelerations during walking. (a) Raw signal. (b) Calibrated accelerations. (c) Lowpass filtered accelerations. (Red color: *X*-axis; Green color: *Y*-axis; Blue color: *Z*-axis.)

where $\mathbf{S}_c$ represents the calibrated accelerations ($\mathbf{A}_c = \left[\, a_{cx}\ a_{cy}\ a_{cz} \,\right]^T$) or angular velocities ($\boldsymbol{\omega}_c = \left[\, \omega_{cx}\ \omega_{cy}\ \omega_{cz} \,\right]^T$). $\mathbf{S}_r$ is the raw accelerations ($\mathbf{A}_r = \left[\, a_{rx}\ a_{ry}\ a_{rz} \,\right]^T$) or angular velocities ($\boldsymbol{\omega}_r = \left[\, \omega_{rx}\ \omega_{ry}\ \omega_{rz} \,\right]^T$) before the calibration procedure. $\mathbf{SF} = \begin{bmatrix} SF_x & 0 & 0 \\ 0 & SF_y & 0 \\ 0 & 0 & SF_z \end{bmatrix}$ and $\mathbf{O} = \left[\, O_x\ O_y\ O_z \,\right]^T$ are the scale factor and offset of the triaxial accelerometer or gyroscope. The more detailed information for the calibration procedures of the accelerometer and gyroscope can be found in [12] and [33]. Fig. 5(a) and (b) show the triaxial accelerations before and after the calibration procedure, respectively. When the triaxial accelerometer is stationary, the measurement of the Z-axis of the triaxial accelerometer, which was placed downward to align with the Earth's gravity, should be equal to -1 g, and the measurements of the X- and Y-axis of the accelerometer should be zero. From Fig. 5(a), the measurement of the X axis of the accelerometer before the calibration is not equal to zero, but that equals to zero after the calibration, as shown in Fig. 5(b). Obviously, the calibrated accelerations are more accurate than the uncalibrated ones.

2) LOWPASS FILTERING

Although the effort to remove the sensors' error sources can be performed through the calibration procedure, the calibrated measurements are still contaminated by the high-frequency noise and with users' unconscious trembles and walking friction. Hence, a lowpass filter is usually designed to remove the abovementioned efforts. In this paper, we design a three-order lowpass Butterworth filter with a 12 Hz cutoff frequency to obtain more accurate inertial measurements since the motion frequency of the lower limbs of humans is usually less than 12 Hz [35]. After the lowpass filtering, we can obtain the lowpass filtered accelerations ($\mathbf{A}_l = \left[\, a_{lx}\ a_{ly}\ a_{lz} \,\right]^T$) and angular velocities ($\boldsymbol{\omega}_l = \left[\, \omega_{lx}\ \omega_{ly}\ \omega_{lz} \,\right]^T$). The triaxial lowpass filtered accelerations are shown as Fig. 5(c). Obviously, the unfiltered accelerations generated by the foot movement include signal spikes which are the noise induced by users' unconscious trembles and walking friction, as shown in Fig. 5(b). However, the signal spikes of the accelerations can be effectively eliminated via the proposed lowpass filter, as shown in Fig. 5(c).

B. GAIT PHASE DETECTION

The proposed gait phase detection algorithm is developed to automatically acquire the gait information of each gait cycle from the lowpass filtered angular velocities generated from the walking motions. The proposed gait phase detection algorithm is composed of the steps described as follows.

Step 1 (Calculation of Signal Vector Magnitude (SVM): The SVM of the filtered angular velocities measured by the triaxial gyroscope is calculated as equation (2).

$$SVM_\omega(k) = \sqrt{\omega_{lx}(k)^2 + \omega_{ly}(k)^2 + \omega_{lz}(k)^2}, \tag{2}$$

where k is the time step, $\omega_{lx}(k)$, $\omega_{ly}(k)$, and $\omega_{lz}(k)$ are the filtered angular velocities of X-, Y-, and Z-axis of the triaxial gyroscope. The filtered angular velocities and its SVM are shown in Fig. 6.

Step 2 (Finding Toe-Off Points of Strides): In general, the SVM of the filtered angular velocities is not zero or relatively large when the foot is at toe-off in the swing phase. However, sudden spikes in the angular velocities during human walking may be revealed during the stance phase. Hence, a simple threshold algorithm of the SVM of the angular velocities is not sufficient to accurately detect the toe-off points within the gait cycle. Therefore, a threshold of a timer is needed to be utilized to circumvent this problem, that is, the sudden spikes of the angular velocities generated from the users' unconscious trembles and walking friction will be ignored. Two parameters, the slope of the SVM and a sample timer, are monitored and used to detect the toe-off points during the walking motions. Firstly, an empirical slope threshold for the

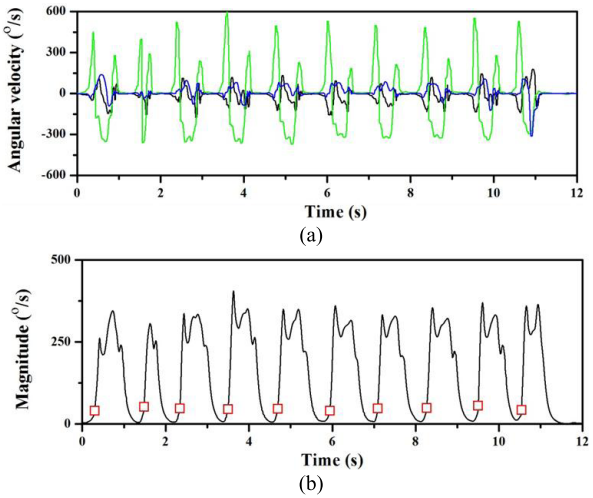

FIGURE 6. Gait phase detection algorithm (a) Filtered angular velocity (Black color: *X*-axis; Green color: *Y*-axis; Blue color: *Z*-axis.) (b) SVM of the filtered angular velocity. Square shape: toe-off points.

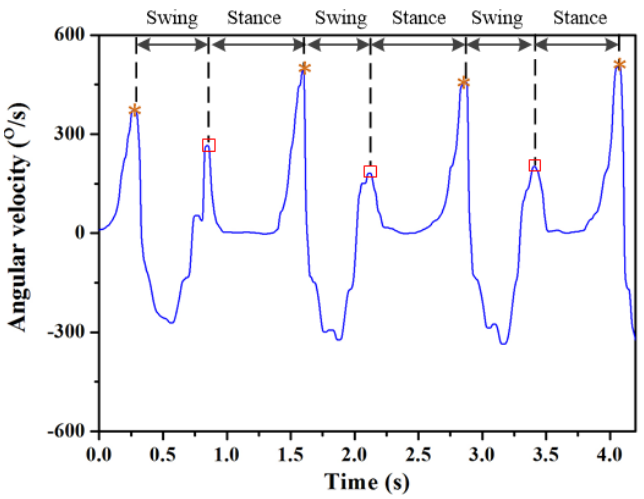

FIGURE 7. Partition of stance phases and swing phases detected by using the SVM and *Y*-axis angular velocity signals of the gyroscope, respectively Square shape: heel-strike points. Star shape: toe-off points.

SVM of the filtered angular velocities is set at 50 °/s to find the candidates for the toe-off points of the gait cycle. That is, once the slopes of the SVM of the filtered angular velocities is higher than the threshold, the present sample points can be designated as the candidates for the toe-off points within the gait cycle. Subsequently, a threshold of the timer is set at 20 sample points (200 ms) to avoid the influence of users' unconscious foot trembles and walking friction, and search out the true toe-off points of the gait cycle from the candidates of the toe-off points. That is, once a toe-off point within a gait cycle is determined, the sudden spikes of the SVM of the angular velocities within the successive 20 sample points will be ignored, which are generated from the users' unconscious trembles and walking friction. As a result, the stance and swing phases will be exchanged when the SVM of the angular velocities has been above or below the slope threshold for a specified time period. Fig. 6(b) shows the SVM of the angular velocities and the detected toe-off points.

Step 3 (Finding Heel-Strike Points of Strides): Once each toe-off point of each stride is detected by using the SVM of the angular velocities, we can further detect the heel-strike point within each stride by using filtered *Y*-axis angular velocities measured by the gyroscope embedded in the foot-mounted IMS module. According to the approach proposed in [14] and [28], we can find out the second local minimums/maximums of the angular velocity in the gait cycle for detecting the heel-strike points. From Fig. 7, the toe-off points are detected by using the SVM of the angular velocities and then each local maximum within the interval of each two successive toe-off points is defined as a heel-strike point within each stride. Once the toe-off and heel-strike points of each gait cycle are found, we can obtain the stance and swing phases. Therefore, the stance time and swing time of each gait cycle can be calculated, respectively.

Step 4 (Calculation of Gait Parameters): Once the toe-off and heel-strike points of each gait cycle are found, we can calculate the following gait parameters to represent the pace and rhythm factors. The gait parameters will be described as follows.

(1) No. of strides: Once the stance and swing phases of the gaits have been determined, the number of strides can be calculated and is expressed in count.

(2) Stride time: The time interval between two successive toe-off points (or heel-stride points) and is expressed in second.

(3) Walking time: The summation of the time of strides and is expressed in second.

(4) Stride length: It is calculated by dividing the number of strides by 10 and is expressed in meter.

(5) Stride frequency: It is calculated by the Fourier transform of the angular velocity signals and is expressed in Hertz (Hz).

(6) Stride velocity: It is calculated by multiplying the stride length and stride frequency and is expressed in meter per second.

(7) Stride cadence: It is calculated by dividing the walking time by number of strides and is expressed in stride per minute.

(8) Stance time: The time interval from the heel-strike point to the toe-off point within each gait cycle and is expressed in second.

(9) Swing time: The time interval from the toe-off point to the heel-strike point within each gait cycle and is expressed in second.

C. ANKLE RANGE OF MOTION ESTIMATION

Once we obtain the filtered accelerations and angular velocities measured from the foot-mounted IMS during walking, the angle of the ankle joint of user's movement can be estimated via a complementary filter. As shown in Fig. 8, the pitch angle, the rotation angle of the *Y*-axis in the sagittal

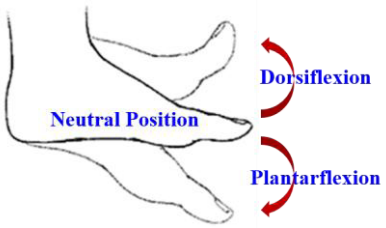

FIGURE 8. The plantarflexion and dorsiflexion angles of ankle.

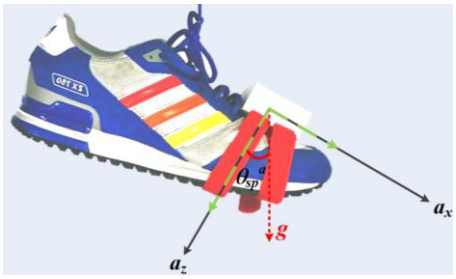

FIGURE 9. Using the lowpass filtered accelerations to estimate the foot angle in the sagittal plane.

plane, can be calculated to be as the ankle ROM (plantarflexion and dorsiflexion angles), which are the important gait patterns for the patients with stroke or Parkinson's disease during walking [1], [10], [15]. Generally, the pitch angle in the sagittal plane can be calculated through the single integral of the filtered Y-axis angular velocity signals measured by the gyroscope during walking in equation (3) [16].

$$\theta^{\omega}_{sp}(k) = \theta^{\omega}_{sp}(k-1) + \frac{1}{2}\Delta k(\omega_{ly}(k) + \omega_{ly}(k-1)), \quad (3)$$

where k and $k-1$ are the present and preceding time steps, ω_{ly} is the filtered Y-axis angular velocity, θ^{ω}_{sp} is the ankle ROM in the sagittal plane calculated by the filtered Y-axis angular velocities. However, the integral of the drift generated from the gyroscope in the low frequency motion causes a cumulative pitch angle error that is extremely large over time. On the other hand, the pitch angle in the sagittal plane can be obtained by the filtered acceleration via the trigonometric operation directly as shown in Fig. 9 and is defined as equation (4).

$$\theta^{a}_{sp}(k) = \tan^{-1}\left(\frac{a_{lx}(k)}{a_{lz}(k)}\right), \quad (4)$$

where k is the time step, a_{lx} and a_{lz} are the filtered X- and Z-axis accelerations, respectively, θ^{a}_{sp} is the ankle ROM in the sagittal plane calculated by the filtered acceleration. Note that, the acceleration signal contains both the gravitational acceleration and the walking accelerations. The walking accelerations generated from the walking motion in the high frequency motion will cause the error of the pitch angle calculation when we utilize the accelerometer to estimate the pitch angle. The abovementioned phenomenon shows that when the accelerometer is used to estimate the pitch angle in high frequency motion, the estimated pitch angle is inaccurate. Fortunately, the pitch angle has more reliable in high frequency motion compared to low frequency motion since its drift problem. Hence, a complementary filter is utilized to accurately estimate the pitch angle in the sagittal plane by fusing the filtered accelerations and angular velocities, which have complementary frequency information [11]. The proposed complementary filter is composed of a lowpass filter and a highpass filter which are located after the trigonometric operation of the filtered acceleration and the integral operation of the filtered Y-axis angular velocity, respectively. The block diagram of the complementary filter is shown in Fig. 4.

In this paper, we design a first order complementary filter to estimate the pitch angle in the sagittal plane (θ_{sp}) as equation (5).

$$\theta_{sp} = H_1\theta^{\omega}_{sp}(k) + H_2\theta^{a}_{sp}(k) = \alpha\theta^{\omega}_{sp}(k) + (1-\alpha)\theta^{a}_{sp}(k), \quad (5)$$

where k is the time step, θ_{sp} is the estimated pitch angle in the sagittal plane via the proposed complementary filter, H_1 and H_2 are the highpass filter and lowpass filter located after the filtered Y-axis angular velocity and acceleration, respectively. Therefore, the complementary filter can be considered as a simple filter by weighting the pitch angles calculated by the angular velocity and acceleration, respectively [23]. α is the turning parameter and can be utilized to allow the pitch angle integrated by the filtered Y-axis angular velocity in the dynamic motion situation to pass through the highpass filter. Conversely, $(1-\alpha)$ can allow the pitch angle calculated by the filtered acceleration in the static or quasi-static motion situations to pass through the lowpass filter. In this paper, according to our empirical tests, we set $\alpha = 0.95$. The time constant (τ) of the complementary filter can be calculated by equation (6).

$$\tau = \frac{\alpha\Delta T}{1-\alpha}, \quad (6)$$

where $\alpha = 0.95$, $\Delta T = 0.01$ sec is the sampling time, and $\tau = 0.19$ sec can be calculated based on (6). That is, when the time period of the walking motion is slower than the time constant (0.19 sec), the weighting of the pitch angle obtained by the filtered acceleration (θ^{a}_{sp}) is more than that of the pitch angle calculated by the gyroscope integration (θ^{ω}_{sp}) to reduce the drift of the gyroscope. The pitch angle changes in the sagittal plane estimated by the complementary filter during walking motion are shown in Fig. 10. Once the compensated pitch angle of each gait cycle can be found, we could distinguish the complete gait cycle through the compensated pitch angle, as shown in Fig. 11. Then, we can calculate the following gait parameters:

(1) $\theta_{sp,rms}$*:* The root mean square (RMS) of the pitch angles (θ_{sp}) in the sagittal plane in each gait cycle

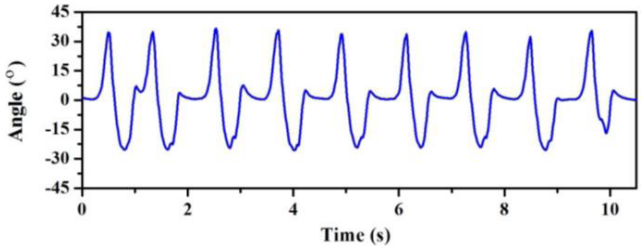

FIGURE 10. Pitch angle changes in the sagittal plane during walking motion.

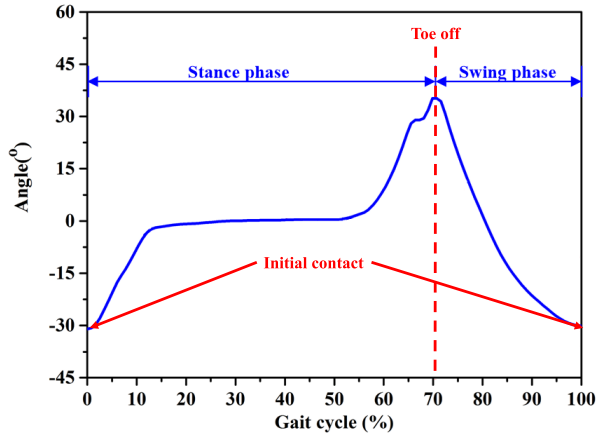

FIGURE 11. Pitch angle changes in the sagittal plane during an entire gait cycle.

as equation (7).

$$\theta_{sp,rms} = \sqrt{\frac{\sum_{k=1}^{N} \theta_{sp}(k)^2}{N}}, \tag{7}$$

where k is the time step and N is the number of the sampling points in each gait cycle.

(2) $\theta_{sp,max}$*:* The maximal value of the pitch angle in the sagittal plane in each gait cycle.

(3) $\theta_{sp,min}$*:* The minimal value of the pitch angle in the sagittal plane in each gait cycle.

IV. EXPERIMENTAL RESULTS AND DISCUSSION

A. SYSTEM VALIDATION

To validate the accuracy of the proposed spatiotemporal gait analysis algorithm for the heel-strike and toe-off point detection, the results obtained from the algorithm are compared with those obtained using two force sensors (FSR406; FlexiForce®), shown in Fig. 12, of size 54.1 mm × 18.3 mm × 0.46 mm, which are attached at the sole on the shoes during walking tests. Fig. 13(a) shows the SVM of the angular velocity signal measured from the gyroscope and the force signal generated by the force sensor attached on tiptoe (FSR_{toe}). The toe-off points (∗) detected from the SVM of the angular velocity signal measured by the gyroscope with the gait phase detection algorithm and those obtained from the force sensor are marked. Fig. 13(b) shows the Y-axis angular velocity signal measured from the gyroscope

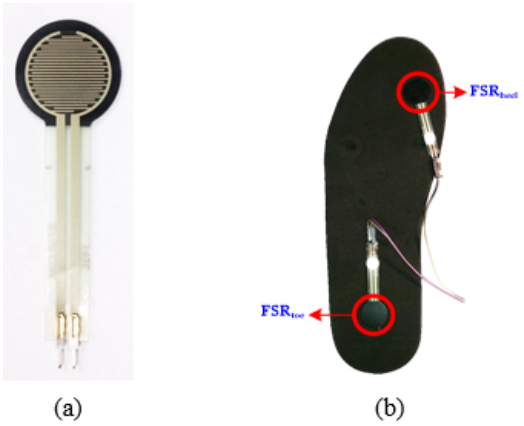

FIGURE 12. The force sensor used for the evaluation of inertial-sensor-based wearable device. (a) FSR406; FlexiForce®. (b) The positions of the force sensor in the insoles.

TABLE 3. The averaged RMSEs for toe-off and heel-strike points obtained during walking (Unit: sec).

Algorithm	Toe-off	Heel-strike
Proposed Method	0.125±0.010	0.089±0.015
Walking step-peak detection [18]	0.290±0.060	0.326±0.071
EC and IC detection [14]	0.055±0.019	0.139±0.186

and the force signal generated by the force sensor attached on heel (FSR_{heel}). Based on the gait phase detection algorithm, the second local maximum of the angular velocity signal within each gait cycle is the heel-strike point. The heel-strike points (■) detected from the gyroscope with the gait phase detection algorithm and those obtained from the force sensor are marked. To evaluate the accuracy of the detection of the toe-off and the heel-strike points, the root mean square error (RMSE) are computed as the averaged difference between the time points detected by the proposed algorithm and those obtained from the force sensors as equation (8).

$$RMSE = \sqrt{\frac{\sum_{k=1}^{N} (FS(k) - GS(i))^2}{N}}, \tag{8}$$

where FS and GS note the toe-off (or heel-strike) point estimated by the force sensors and the gyroscope with the gait phase detection algorithm, respectively. N is the number of strides during walking. In addition, we implemented two gait event detection algorithms presented in [14] and [18], and the results obtained from the algorithms are compared with those obtained the proposed spatiotemporal gait analysis algorithm. According to Table 3, we found out that our approach gives quite accurate estimation of both time points of toe-off and heel-strike, with averaged RMSEs of 0.125±0.010 s for toe-off points and 0.089±0.015 s for heel-strike points during walking. However, the averaged RMSEs for toe-off points and heel-strike points are 0.290±0.060 s and 0.326±0.071 s by the approach of [18] and 0.055±0.019 s and 0.139±0.186 s by the approach of [14].

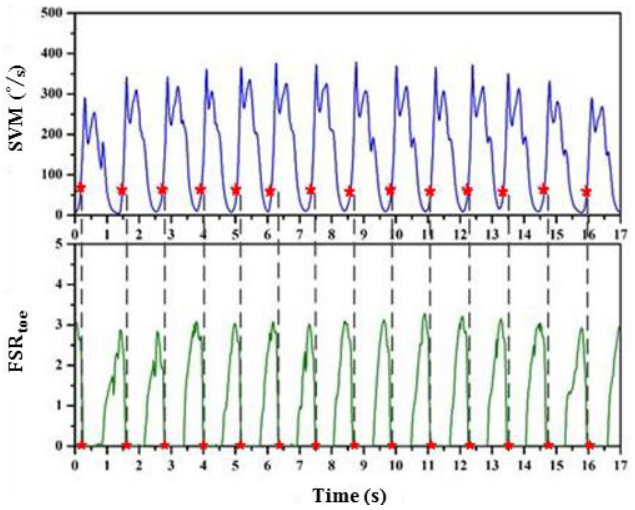

(a)

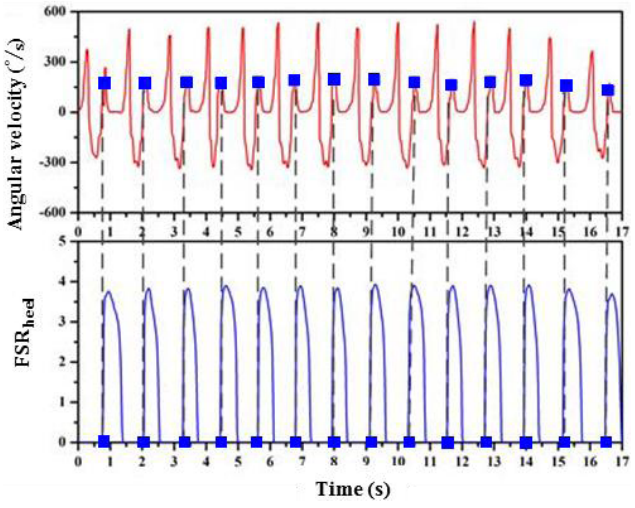

(b)

FIGURE 13. (a) SVM of the angular velocity signal measured from the gyroscope using the proposed gait phase detection algorithm (the upper figure) and the force signal generated by the force sensor attached on toe (FSR_{toe}) (the lower figure). Star (∗) indicate the toe-off points detected by the proposed algorithm and the force sensor. (b) Angular velocity signal measured from the *Y*-axis gyroscope using the proposed gait phase detection algorithm (the upper figure) and the force signal generated by the force sensor attached on heel (FSR_{heel}) (the lower figure). Square (■) indicate the heel-strike points detected by the proposed algorithm and the force sensor.

B. GAIT ANALYSIS FOR PATIENTS WITH STROKE

The walking ability of patients with stroke is related to the degree of functional recovery. In this paper, each stroke participant were asked to walk along a straight line of 10 m for examining the relationship between the walking gait parameters and the degree of motor recovery after stroke. In the 10 m walking test, each stroke participant were asked to repeat the walking trails one more time after an interval, over a period of 2 min. The spatiotemporal gait parameters for each of the stroke patients and HCs when walking at self-selected speeds in the 10 m walking test are shown in Table 4. The statistical results of gait parameters showed significant differences (p-value < 0.05) between the stroke and HC groups.

TABLE 4. Gait parameters of stroke and HC groups in walking test.

Parameters	Stroke N = 4	HC N = 15	p-value
No. of strides (count)	10.86±4.30	7.73±1.16	0.014*
Stride time (sec)	1.69±0.55	1.02±0.06	<0.001***
Walking time (sec)	16.84±5.52	7.55±1.22	<0.001***
Stride length (m)	1.03±0.33	1.33±0.19	0.013*
Stride frequency (Hz)	0.64±0.17	0.99±0.06	<0.001***
Stride velocity (m/sec)	0.66±0.24	1.32±0.21	<0.001***
Stride cadence (stride/min)	38.37±10.24	61.19±3.60	<0.001***
Stance time (sec)	1.09±0.38	0.57±0.04	<0.001***
Swing time (sec)	0.59±0.18	0.46±0.03	0.007**
θ_{sp}_RMS	6.28±4.69	12.56±1.97	0.004**
$\theta_{sp,max}$ (°)	21.18±15.59	39.22±7.28	0.009**
$\theta_{sp,min}$ (°)	-16.32±11.55	-28.98±4.25	0.012*

*p <0.05, **p <0.01, ***p <0.001

Obviously, the stroke patients needed more stride counts, stride time, and walking time to complete the 10 m walking test. The stroke patients presented significantly shorter stride length, lower stride frequency, slower stride velocity, lower stride cadence, longer stance time, and longer swing time in comparison with the HCs. The finding in some previous studies also indicated that the stroke patients demonstrated a shorter stride length, a slower stride velocity, a lower stride cadence, a longer stride time, a longer stance time, and a longer swing time compared with the HCs when walking at self-selected speeds [2], [15], [22], [30]. This abovementioned notable phenomenon presumably indicates that the stroke patients have difficulty walking faster to complete the walking task due to weakness of foot drop and extensor hypertonia in their lower limbs. Another finding in the walking test is that the stroke patients spent more time in the stance time and swing time compared with the HCs in this paper, which could be explained by the inference that stroke patients needed more time in their double limb support period to compensate for their weak leg muscle power and to maintain balance. This notable phenomenon presumably indicates that the stroke patients exhibited increased time for standing to compensate for the decreased of their balance so as to control stability between steps [15].

The pattern and magnitude of the ankle ROM in the sagittal plane of the HCs and stroke patients during entire gait cycle are showed in Fig. 14. Obviously, the movement patterns in the sagittal plane sinusoidal curve of ankle are similar to both groups. However, the HCs' ankle ROM is much larger than that of the stroke patients, with a mean 6.28 beyond for $\theta_{sp,rms}$, a mean 18.04° beyond for $\theta_{sp,max}$, and a mean 12.66° beyond for $\theta_{sp,min}$. Additionally, Fig. 14 shows some symptoms of gait patterns of the stroke patients: (1) the angle magnitude was decreased at initial contact because of the foot is nearly flat; (2) the ankle plantarflexion was decreased at toe off; (3) the decreased abnormal control of the ankle dorsiflexion results in the reduced ankle angle magnitude. The finding in some previous studies also indicated that the stroke patients demonstrated a smaller ankle plantarflexion, a smaller ankle dorsiflexion, and a smaller foot angle com-

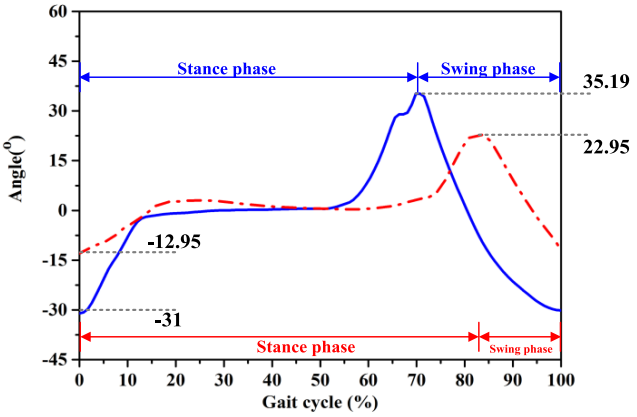

FIGURE 14. Sagittal plane angles of gait cycle from a HC and a stroke subject. (Blue color: HC. Red color: Hemiplegia subject.)

pared with the HCs during normal walking [10]. This notable phenomenon presumably indicates that the stroke patients exhibited circumduction gait to compensate for the insufficient ankle dorsiflexion of affected limb. Some previous literatures also reported that the stroke patients often used limb vaulting to assist limb clearance, which results in an increased foot lateral displacement during swing phase in the affected limb [5], [15].

The abovementioned results agree with some previous studies in stroke patients using other motion analysis systems, such as Vicon® motion analysis system [15] and OrthoTrack motion analysis system [2]. Therefore, the proposed foot-mounted IMS and its associated spatiotemporal gait analysis algorithm can extract some of the spatiotemporal gait characteristics to discriminate between the HC and stroke groups effectively.

C. GAIT ANALYSIS FOR PATIENTS WITH PARKINSON'S DISEASE

Table 5 summarizes the results of the PD and HC groups in the 10 m walking test. PD group differed significantly from the HC group on number of strides, walking time, stride length, and stride velocity. Reduced stride velocity is a common symptom of bradykinesia in PD patients, which causes that the PD patients need more stride counts and walking time to complete the 10 m walking test. In addition, the PD patients presented shorter stride length in comparison with the HCs since they walked with increased double support duration [20]. Some previous literatures also reported that the stride velocity and stride length revealed significant differences in a walking test in PD subjects [1], [17], [25], [27], [29], [30]. In addition, the results also appeared to have lower stride frequency and lower stride cadence, but these characteristics were not significant. The gait profiles are consistent with that found in some previous studies [7], [17], [27]. Additionally, Fig. 15 shows that the walking patterns of the PD patients are similar to that of the HC group. The $\theta_{sp,rms}$, $\theta_{sp,max}$, and $\theta_{sp,min}$ in the sagittal plane had significant

TABLE 5. Gait parameters of PD and HC groups in walking test.

Parameters	PD N = 5	HC N = 15	*p*-value
No. of strides (count)	10.00±2.92	7.73±1.16	0.002**
Stride time (sec)	1.02±0.05	1.02±0.06	0.992
Walking time (sec)	9.80±2.59	7.55±1.22	0.015*
Stride length (m)	1.07±0.26	1.33±0.19	0.025*
Stride frequency (Hz)	0.98±0.05	0.99±0.06	0.646
Stride velocity (m/sec)	1.04±0.24	1.32±0.21	0.023*
Stride cadence (stride/min)	60.42±3.19	61.19±3.60	0.678
Stance time (sec)	0.57±0.03	0.57±0.04	0.906
Swing time (sec)	0.45±0.02	0.46±0.03	0.854
θ_{sp}_RMS	7.41±0.15	12.56±1.97	<0.001***
$\theta_{sp,max}$ (°)	32.93±0.03	39.22±7.28	0.006**
$\theta_{sp,min}$ (°)	-19.23±0.39	-28.98±4.25	<0.001***

*p <0.05, **p <0.01, ***p <0.001.

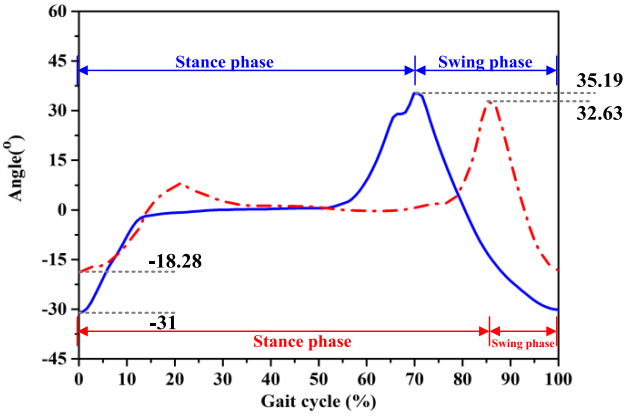

FIGURE 15. Sagittal plane angles of gait cycle from a HC and a PD subject. (Blue color: HC. Red color: PD.)

differences between the PD patients and HCs. The HCs' ankle ROM is much larger than that of the PD patients, with a mean 5.15 beyond for $\theta_{sp,rms}$, a mean 6.29° beyond for $\theta_{sp,max}$, and a mean 9.75° beyond for $\theta_{sp,min}$. The findings in some previous studies indicated that the PD subjects demonstrated reduced ankle plantarflexion and dorsiflexion angles and consisted of a reduction in ROM in swing phase [1], [27].

V. CONCLUSIONS

In this study, a systematic framework of the gait analysis for the patients with stroke or Parkinson's disease has been presented. We analyzed the acquired gait parameters in order to determine different characteristics in gait profiles between the stroke patients, PD patients, and HCs. A wearable IMS with its associated spatiotemporal gait analysis algorithm has been developed for recording inertial signals generated from walking movement without any external device and analyzing gait parameters for evaluation of walking ability automatically. Through trials of 10 m walking test, the proposed wearable device demonstrated its effective capability to measure spatial and temporal gait parameters, and to estimate ankle ROMs. Experimental results indicated that

stroke patients showed significantly impaired gait profiles and sagittal kinematic waveforms compared with HCs, which could be utilized to assess gait disorders and evaluate the recovery situation of walking capacity for stroke patients during their rehabilitation courses. On the other hand, number of strides, walking time, stride length, stride velocity, RMS of the pitch angles, maximal value of the pitch angle, and minimal value of the pitch angle in the sagittal plane may be defined as key features for discrimination of PD patients from healthy elderly. In the present study, the gait profiles in the sagittal plane of the ankle joint were extracted. Although the presented gait profiles could be as discriminative features between the stroke patients, PD patients, and HCs, future extension of this study should use more sensors to obtain knee and hip angles for the evaluation of gait pathology in coronal and horizontal planes [15], [27]. The advantages of this approach include the following: 1) with the IMS, the patients' gait information can be measured and evaluated in naturalistic environments without space limitation; 2) the complementary filter can effectively reduce the integration errors of inertial signals for estimating more accurate ankle ROMs; and 3) the proposed IMS is a promising device in obtaining insightful gait information of patients with stroke and PD. The results presented in this paper suggest that the inertial-sensor-based wearable device reveals promising potential for gait analysis and is worth of further in-depth research to identify gait parameters in stroke or PD patients, so as to be served as indicators for discrimination of stroke or PD patients from healthy elderly, and also as an assessment indicator of therapeutic efficacy during rehabilitation.

REFERENCES

[1] S. J. M. Bamberg, A. Y. Benbasat, D. M. Scarborough, D. E. Krebs, and J. A. Paradiso, "Gait analysis using a shoe-integrated wireless sensor system," *IEEE Trans. Inf. Technol. Biomed.*, vol. 12, no. 4, pp. 413–423, Jul. 2008.

[2] J. Boudarham, N. Roche, D. Pradon, C. Bonnyaud, D. Bensmail, and R. Zory, "Variations in kinematics during clinical gait analysis in stroke patients," *PLoS ONE*, vol. 8, no. 6, pp. 1–9, 2013.

[3] J. Barth *et al.*, "Stride segmentation during free walk movements using multi-dimensional subsequence dynamic time warping on inertial sensor data," *Sensors*, vol. 15, no. 3, pp. 6419–6440, 2015.

[4] N. C. Bejarano, E. Ambrosini, A. Pedrocchi, G. Ferrigno, M. Monticone, and S. Ferrante, "A novel adaptive, real-time algorithm to detect gait events from wearable sensors," *IEEE Trans. Neural Syst. Rehabil. Eng.*, vol. 23, no. 3, pp. 413–422, May 2015.

[5] G. Chen, C. Patten, D. H. Kothari, and F. E. Zajac, "Gait differences between individuals with post-stroke hemiparesis and non-disabled controls at matched speeds," *Gait Posture*, vol. 22, no. 1, pp. 51–56, 2005.

[6] E. R. Dorsey *et al.*, "Projected number of people with Parkinson disease in the most populous nations, 2005 through 2030," *Neurology*, vol. 68, no. 5, pp. 384–386, 2007.

[7] M. Demonceau *et al.*, "Contribution of a trunk accelerometer system to the characterization of gait in patients with mild-to-moderate Parkinson's disease," *IEEE J. Biomed. Health Informat.*, vol. 19, no. 6, pp. 1803–1808, Nov. 2015.

[8] S. D. Din, A. Godfrey, and L. Rochester, "Validation of an accelerometer to quantify a comprehensive battery of gait characteristics in healthy older adults and Parkinson's disease: Toward clinical and at home use," *IEEE J. Biomed. Health Informat.*, vol. 20, no. 3, pp. 838–847, May 2016.

[9] R. J. Ellis *et al.*, "A validated smartphone-based assessment of gait and gait variability in Parkinson's disease," *PLoS ONE*, vol. 10, no. 10, pp. 1–22, 2015.

[10] Y. Guo, D. Wu, G. Liu, G. Zhao, B. Huang, and L. Wang, "A low-cost body inertial-sensing network for practical gait discrimination of hemiplegia patients," *Telemed. e-Health*, vol. 18, no. 10, pp. 748–754, 2012.

[11] M. Ghanbari and M. J. Yazdanpanah, "Delay compensation of tilt sensors based on MEMS accelerometer using data fusion technique," *IEEE Sensors J.*, vol. 15, no. 3, pp. 1959–1966, Mar. 2015.

[12] Y.-L. Hsu, C.-L. Chu, Y.-J. Tsai, and J.-S. Wang, "An inertial pen with dynamic time warping recognizer for handwriting and gesture recognition," *IEEE Sensors J.*, vol. 15, no. 1, pp. 154–163, Jan. 2015.

[13] M. Iosa *et al.*, "Assessment of upper-body dynamic stability during walking in patients with subacute stroke," *J. Rehabil. Res. Develop.*, vol. 49, no. 3, pp. 439–450, 2012.

[14] J. M. Jasiewicz *et al.*, "Gait event detection using linear accelerometers or angular velocity transducers in able-bodied and spinal-cord injured individuals," *Gait Posture*, vol. 24, no. 4, pp. 502–509, 2006.

[15] J. Kim *et al.*, "Gait patterns of chronic ambulatory hemiplegic elderly compared with normal age-matched elderly," *Int. J. Precis. Eng. Manuf.*, vol. 16, no. 2, pp. 385–392, 2015.

[16] T. Liu, Y. Inoue, and K. Shibata, "Development of a wearable sensor system for quantitative gait analysis," *Measurement*, vol. 42, no. 7, pp. 978–988, 2009.

[17] K. A. Lowry, A. L. Smiley-Oyen, A. J. Carrel, and J. P. Kerr, "Walking stability using harmonic ratios in Parkinson's disease," *Movement Disorders*, vol. 24, no. 2, pp. 261–267, Jan. 2009.

[18] J.-A. Lee, S.-H. Cho, Y.-J. Lee, H.-K. Yang, and J.-W. Lee, "Portable activity monitoring system for temporal parameters of gait cycles," *J. Med. Syst.*, vol. 34, no. 5, pp. 959–966, 2010.

[19] H.-T. Li, J.-J. Huang, C.-W. Pan, H.-I. Chi, and M.-C. Pan, "Inertial sensing based assessment methods to quantify the effectiveness of post-stroke rehabilitation," *Sensors*, vol. 15, no. 7, pp. 16196–16209, 2015.

[20] M. E. Morris, R. Iansek, T. A. Matyas, and J. J. Summers, "Stride length regulation in Parkinson's disease: Normalization strategies and underlying mechanisms," *Brain*, vol. 119, pp. 551–568, Apr. 1996.

[21] S. J. Morris, "A shoe-integrated sensor system for wireless gait analysis and real-time therapeutic feedback," Ph.D. dissertation, Dept. Harvard/MIT Div. Health Sci. Technol., Cambridge, MA, USA, 2004.

[22] C. Mizuike, S. Ohgi, and S. Morita, "Analysis of stroke patient walking dynamics using a tri-axial accelerometer," *Gait Posture*, vol. 30, no. 1, pp. 60–64, 2009.

[23] B. Muset and S. Emerich, "Distance measuring using accelerometer and gyroscope sensors," *Carpathian J. Electron. Comput. Eng.*, vol. 5, no. 1, pp. 83–86, 2012.

[24] A. Mannini, D. Trojaniello, A. Cereatti, and A. M. Sabatini, "A machine learning framework for gait classification using inertial sensors: Application to elderly, post-stroke and Huntington's disease patients," *Sensors*, vol. 16, no. 1, p. 134, 2016.

[25] A. Peppe, C. Chiavalon, P. Pasqualetti, D. Crovato, and C. Caltagirone, "Does gait analysis quantify motor rehabilitation efficacy in Parkinson's disease patients?" *Gait Posture*, vol. 26, no. 3, pp. 452–462, 2007.

[26] S. Rezvanian and T. E. Lockhart, "Towards real-time detection of freezing of gait using wavelet transform on wireless accelerometer data," *Sensors*, vol. 16, no. 4, p. 475, 2016.

[27] O. Sofuwa, A. Nieuwboer, K. Desloovere, A. M. Willems, F. Chavret, and I. Jonkers, "Quantitative gait analysis in Parkinson's disease: Comparison with a healthy control group," *Arch. Phys. Med. Rehabil.*, vol. 86, no. 5, pp. 1007–1013, 2005.

[28] A. M. Sabatini, C. Martelloni, S. Scapellato, and F. Cavallo, "Assessment of walking features from foot inertial sensing," *IEEE Trans. Biomed. Eng.*, vol. 52, no. 3, pp. 486–494, Mar. 2005.

[29] D. Trojaniello *et al.*, "Estimation of step-by-step spatio-temporal parameters of normal and impaired gait using shank-mounted magneto-inertial sensors: Application to elderly, Hemiparetic, Parkinsonian and choreic gait," *J. NeuroEng. Rehabil.*, vol. 11, p. 152, 2014.

[30] D. Trojaniello, A. Ravaschio, J. M. Hausdorff, and A. Cereatti, "Comparative assessment of different methods for the estimation of gait temporal parameters using a single inertial sensor: Application to elderly, post-stroke, Parkinson's disease and Huntington's disease subjects," *Gait Posture*, vol. 42, no. 3, pp. 310–316, 2015.

[31] P. H. Truong, J. Lee, A. R. Kwon, and G.-M. Jeong, "Stride counting in human walking and walking distance estimation using insole sensors," *Sensors*, vol. 16, no. 6, p. 823, 2016.

[32] *Neurological Disorders: Public Health Challenges*, World Health Org., Geneva, Switzerland, 2006.

[33] J.-S. Wang, Y.-L. Hsu, and J.-N. Liu, "An inertial-measurement-unit-based pen with a trajectory reconstruction algorithm and its applications," *IEEE Trans. Ind. Electron.*, vol. 57, no. 10, pp. 3508–3521, Oct. 2010.
[34] *The Top 10 Causes of Death*, World Health Org., Geneva, Switzerland, 2014.
[35] C. Verplaetse, "Inertial proprioceptive devices: Self-motion-sensing toys and tools," *IBM Syst. J.*, vol. 35, nos. 3–4, pp. 639–650, 1996.
[36] S. Yang, J.-T. Zhang, A. C. Novak, B. Brouwer, and Q. Li, "Estimation of spatio-temporal parameters for post-stroke hemiparetic gait using inertial sensors," *Gait Posture*, vol. 37, no. 3, pp. 354–358, 2013.

HSING-CHENG CHANG received the B.S. and M.S. degrees in physics from Tamkang University, Taiwan, in 1978 and 1980, respectively, and the M.S. and Ph.D. degrees in electrical and computer engineering from the University of Cincinnati, Ohio, USA, in 1991 and 1994, respectively.

He is currently a Professor with the Department of Automatic Control Engineering, Feng Chia University, Taiwan. His research interests include microsensors and microactuators, circuit design, automation technology, and engineering education.

YU-LIANG HSU received the B.S. degree in automatic control engineering from the Feng Chia University, Taichung, Taiwan, in 2004, and the M.S. and Ph.D. degrees in electrical engineering from National Cheng Kung University, Tainan, Taiwan, in 2007 and 2011, respectively.

He is currently an Assistant Professor with the Department of Automatic Control Engineering, Feng Chia University, Taiwan. His current research interests include computational intelligence, nonlinear system identification, biomedical signal processing, and inertial sensing applications.

SHIH-CHIN YANG (S'10–M'12) was born in Taiwan. He received the M.S. degree from National Taiwan University, Taiwan, and the Ph.D. degree from the University of Wisconsin-Madison, WI, in 2007 and 2011, respectively. From 2011 to 2015, he was a Research Engineer with Texas Instruments Motor Lab, Dallas, TX, USA.

He is currently an Assistant Professor with National Taiwan University, Taiwan, with the responsibility on the development of motor drive and motor control technology. His research interests include motor drive, power electronics, and control systems. He was a recipient of the IEEE Industry Applications Society Industrial Drive Committee First Prize Paper Award in 2011.

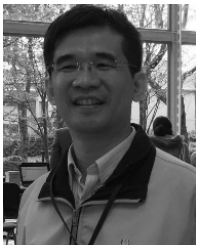

JUNG-CHIH LIN is currently an attending Physician of Department of Integrated Chinese and Western Medicine, Chung Shan Medical University Hospital, College of Medicine, Chung Shan Medical University, Taichung, Taiwan. He is also a Chinese Medicine Doctor and a Pharmacist.

His current research focuses on the fields of neurorehabilitation, stroke rehabilitation, and pain medicine, ingredients, and toxicity analysis of Chinese medicine.

ZHI-HAO WU received the B.S. and M.S. degree in automatic control engineering from the Feng Chia University, Taichung, Taiwan, in 2013 and 2015, respectively.

His research interests include signal processing and human-computer interface.